Available online at www.sciencedirect.com

ScienceDirect

Energy Procedia 92 (2016) 523 – 530

Energy Procedia

6th International Conference on Silicon Photovoltaics, SiliconPV 2016

Optical constants of UV transparent EVA and the impact on the PV module output power under realistic irradiation

Malte R. Vogt[a,*], Hendrik Holst[a], Henning Schulte-Huxel[a], Susanne Blankemeyer[a], Robert Witteck[a], David Hinken[a], Matthias Winter[b], Byungsul Min[a], Carsten Schinke[b], Ingo Ahrens[a], Marc Köntges[a], Karsten Bothe[a], Rolf Brendel[a,b]

[a]*Institute for Solar Energy Research Hamelin (ISFH), Am Ohrberg 1, 31860 Emmerthal, Germany*
[b]*Dep. Solar Energy, Inst. Solid-State Physics, Leibniz Universität Hannover, Appelstr. 2, 30167 Hanover, Germany*

Abstract

We measure and discuss the complex refractive index of conventional ethylene vinyl acetate (EVA) and an EVA with enhanced UV-transmission based on spectroscopic ellipsometry, transmission and reflection measurements over the wavelength range from 300-1200 nm. Ray tracing of entire solar cell modules using this optical data predicts a 1.3% increase in short circuit current density (J_{sc}) at standard test conditions for EVA with enhanced UV transmission. This is in good agreement with laboratory experiments of test modules that result in a 1.4% increase in J_{sc} by using a UV transparent instead of a conventional EVA. Further, ray tracing simulations with realistic irradiation conditions with respect to angular and spectral distribution reveal an even larger J_{sc} increase of 1.9% in the yearly average. This increase is largest in the summer months with an increase of up to 2.3%.

Peer review by the scientific conference committee of SiliconPV 2016 under responsibility of PSE AG.

Keywords: Ray tracing; PV modules; ethylene vinyl acetate (EVA); UV transmission;

* Corresponding author. Tel.: +49-511-762-17253.
E-mail address: m.vogt@isfh.de

Peer review by the scientific conference committee of SiliconPV 2016 under responsibility of PSE AG.
doi:10.1016/j.egypro.2016.07.136

1. Introduction

Module encapsulants that transmit UV light are required to utilize the improved blue response of recent solar cells [1]. In a typical industrial type Si photovoltaic module the absorption in the ethylene vinyl acetate (EVA) encapsulation is the biggest loss factor in the UV wavelength region [2]. Thus the PV modules with the highest power output [3] or efficiencies [4] are encapsulated with UV transparent $EVA_{UV\text{-}T}$. Laboratory experiments performed under standard test conditions (STC) showed a gain of 0.6% to 1% in J_{sc} [3] [5] [6] [7] due to $EVA_{UV\text{-}T}$, compared to conventional UV absorbing EVA_{Conv}.

However, no data for optical constants of UV transparent $EVA_{UV\text{-}T}$ have been published until recently [8]. The absence of such data resulted in a lack of predictions for the energy yield improvement due to $EVA_{UV\text{-}T}$ under realistic irradiation conditions in the field. This work presents how realistic irradiation conditions affect the expected module power output when replacing an EVA_{Conv} with an $EVA_{UV\text{-}T}$. Our ray tracing results show an increase in J_{sc} that is strongest in the summer months.

2. Determination of optical constants

We prepare EVA samples without glass as substrate using Bridgestone EVASKY S87 (UV-T) and S88 (Conv). A sample thickness of 10.2 mm is achieved by laminating a stack of 25 EVA layers. The increased thickness improves the accuracy of the extinction coefficient measurement. The surface roughness is reduced to a minimum since a smother surface simplifies the data analysis of the measurement.

Transmission and reflection measurements are conducted with a Varian Cary 5000 in the wavelength range from 250-2500 nm. The Cary 5000 two-channel spectrophotometer is equipped with an integrating sphere accessory [9]. To improve the measurement accuracy for the real part of the refractive index we, additionally, use spectroscopoic ellipsommetry in the wavelength range from 250-1690 nm. The ellipsometer is commercially available Woollam M-2000UI rotating compensator ellipsometer [10]. For the spectral ellipsometry measurements, the angles of incidence are 50°, 60°, and 70°. The reflection at the rear side is prevented from reaching the detector using a light trap at the rear side of the samples.

For data acquisition and analysis, the WVASE32 software [10] is used. In the data analysis, each sample is modeled with a 1-2 nm thin surface layer to mimic surface roughness: the surface layer's optical constants are

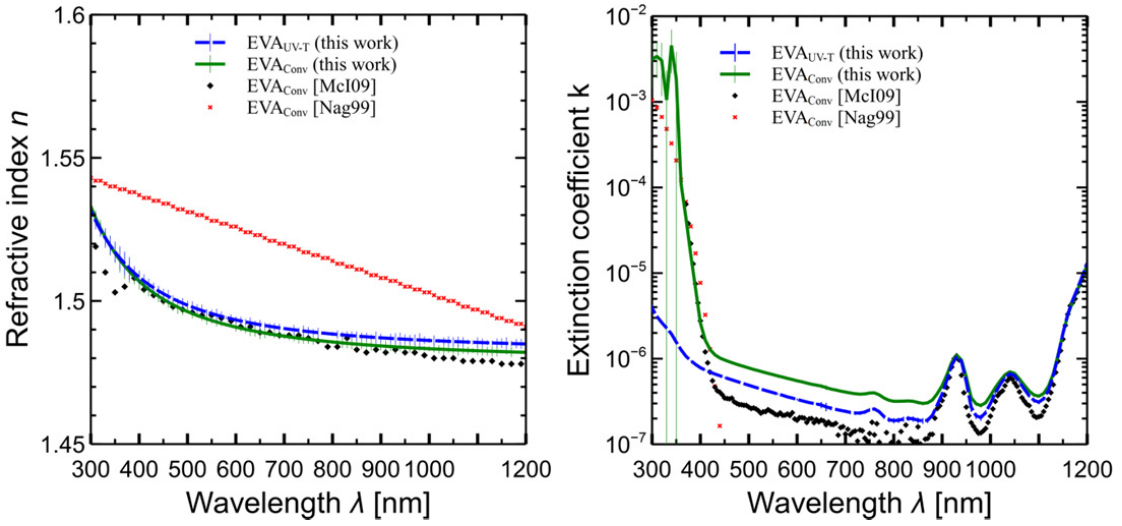

Fig. 1. Real part of the refractive index (left) and extinction coefficient (right) of UV transparent $EVA_{UV\text{-}T}$ from this work (blue, dashed line) and conventional UV absorbing EVA_{Conv} from Nagel et al. [11] (red, crosses), McIntosh et al. [2] (black, diamonds) and this work (green line).

determined by using an effective medium approach [10] assuming 50% EVA and 50% air. This surface layer leads to better agreement between the measured data and our fits. We use a Monte Carlo based iterative fit procedure [12] [13] to determine the accuracy of our $n(\lambda)$ and $k(\lambda)$ results.

The results are depicted for the wavelength range from 300-1200 nm in Fig. 1. For the real part of the refractive index n (left) both of our EVA samples are in agreement with the values from McIntosh et al. [2] for conventional EVA_{Conv}. The measurement uncertainty for the refractive index $n(\lambda)$ is below 3.4% for the $EVA_{UV\text{-}T}$ and 3.8% for the EVA_{Conv} sample.

The extinction coefficients k are shown on the right part of Fig. 1. For wavelengths below 900 nm the UV transparent $EVA_{UV\text{-}T}$ (blue dashed) shows a lower extinction coefficient than the measured conventional EVA_{Conv} sample (green line). All the EVA_{Conv} samples show an increase for the k with decreasing wavelength below 400 nm. This appears to be caused by UV absorbers, which were intentionally added to conventional EVA_{Conv} [14]. Due to the lack of transmission through our 10.2 mm thick sample the measurement uncertainty for the EVA_{Conv} sample is very large below 380 nm. Thus we enhance the accuracy in this spectral range by measuring a thin 1.2 mm sample. The resulting measurement uncertainty is between 50% and 150% in the UV wavelength region. McIntosh et al. [2] did not provide k values below 365 nm due to the high absorption, the k-value of Nagel et al. [10] (red, crosses) for wavelengths below 380 nm lies below our k values. For wavelengths above 380 nm the measurement uncertainty of the EVA_{Conv} sample (green line) is better than 9% and for the $EVA_{UV\text{-}T}$ sample (blue dashed line) it is better than 13%. For more details on the measurement and the uncertainty analysis we refer to ref. [8].

3. Ray tracing and experimental validation at standard test conditions

Conventional EVA_{Conv} is the most commonly used encapsulation material in Si photovoltaics. The EVA with enhanced UV-transmission improves the modules power output, thus we use the above presented data for simulating the photogeneration in a module.

3.1. Ray tracing approach

In Table 1 the geometrical features of the module and the optical constants of all materials (data are available online in the listed references). All materials, except for the well known metals (Ag and Al), were optically characterized by ISFH. The four standard cell interconnection ribbons (CIR), are modeled using the profile extracted from a cross sectional micrograph [15] with width 1.5 mm and height 232 µm. The fingers are modeled using the profile extracted from a scanning electron microscope (SEM) image [16] with a width of 60 µm and a height 18 µm. The solar front glass is a soda lime float glass with Fe_2O_3 weight total of 0.01 ‰ according to model 1 in ref. [13].

Table 1. Module components optical properties and thicknesses as used in experimental test modules and ray tracing simulations.

Module component	Material	Thickness
Glass ARC	Porose glass layer [17]	115 nm
Glass	Low iron float glass [13]	3.2 mm
Encapsulant	EVA [8] (shown in Fig. 1)	450 µm above cells
		190 µm between cells
		450 µm below cells
Connector	Solder alloy [15]	232.4 µm
Finger	Ag [18]	20 µm
Cell front ARC	$SiN_{n=1.9}$ [17]	75 nm
Cell	Si (n [17]; k [12])	170 µm
Cell rear side dielectric	$SiN_{n=1.9}$ [17]	200 nm
Cell full area rear metallization	Al [19]	20 µm
Backsheet	White backsheet [17]	300 µm

We perform a ray tracing simulation that is a good compromise between accuracy and simulation speed. The ray tracing is done in three dimensions using the ray tracing framework DAIDALOS [20]. The ray is traced alternating between three different simulation domains [21] as is shown in Fig. 2 because a module contains features from meters to micrometers.

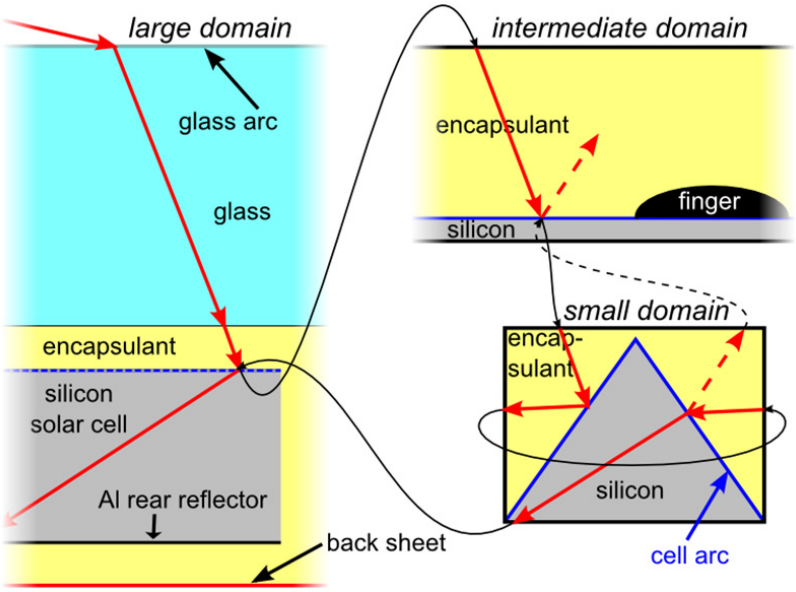

Fig. 2. Multi-domain approach. Left: Large scale domain containing the glass, encapsulation, standard CIR, cells and back sheet. Right top: Intermediate domain containing the fingers. Right bottom: Small domain containing the texture with the cells front ARC.

The rays are generated in the large scale domain, which is constrained by the module front glass, the back sheet and the periodic boundary conditions for the center cells (cells surrounded by other cells thus having no contact with the module frame); it contains the glass cover, the encapsulant, the interconnectors and the cells. If the ray hits the cell's front side, the ray switches to the intermediate scale domain that contains a symmetry element of the cell's fingers. If the ray impinges on silicon, it is transferred to the small scale domain, which contains a single pyramid texture of the cell. Because the approximately 10^{10} pyramids have a random distribution of size and position, the small-scale domain is positioned with a random shift. Once the interaction at the cell's front side is determined the ray (if not absorbed) is transferred back to the large domain.

3.2. Validation of ray tracing model at standard test conditions

For standard test conditions (STC) we model a light source with rays orthogonally incident to the module glas surface and AM1.5G spectrum (IEC 60904-3, Ed. 2.0). The wavelength range is between 300 and 1200 nm and divided in 10 nm steps. We simulate 10 000 rays per wavelength at random positions. From the ray tracing results we calculate the photogenerated current density J_{gen} (λ). This current density is related to the short circuit current density $J_{sc} = \int \eta(\lambda)\, J_{gen}(\lambda)\, d\lambda$ via the collection efficiency $\eta(\lambda)$. We model the semiconductor properties numerically using SENTAURUS [22] to derive the collection efficiency. We select the input parameters to match the characteristics of our PERC solar cell with 20.7% efficiency, which are used for the experimental test modules.

Figure 3 shows the ray tracing results of a module with conventional EVA (left) and with $EVA_{UV\text{-}T}$ (right). The conventional EVA_{Conv} absorbs most of the light in the UV wavelength range below 380 nm, here shown in dark blue. Over the wavelength range from 300 nm to 1200 nm about 2.8% of the photocurrent are parasitically absorbed in the conventional EVA_{Conv}. In contrast, the module with $EVA_{UV\text{-}T}$ (right) reduces this to 1.1% parasitic absorption in the $EVA_{UV\text{-}T}$ with most of the remaining parasitic absorption occurring in the NIR above 1150 nm. However,

integration over all wavelengths results in a gain of (1.3±0.13)% or 0.5 mA/cm² in J_{sc} by using UV transparent instead of conventional EVA_{Conv}. This means other 0.4% of the difference in absorption losses between EVA_{UV-T} and EVA_{Conv} are now increased losses in the back sheet (light green), in the cell ARC (cyan) and losses due to the collection efficiency (pink) this occurs mainly in the UV wavelength region. Consequently, the stability of these components is of stronger concern when fabricating a module with EVA_{UV-T}.

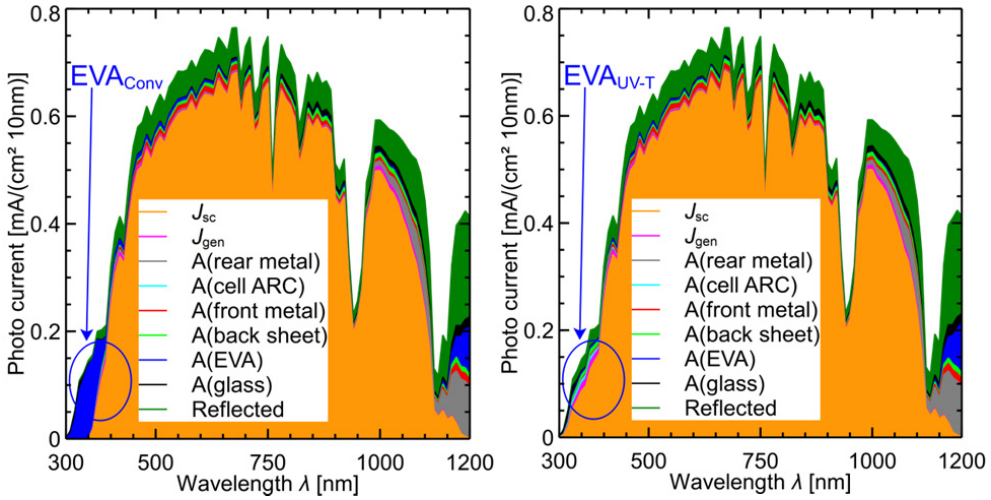

Fig. 3. Optical loss analysis of the PV modules with EVA_{Conv} (left) and EVA_{UV-T} (right) both under normal incident and AM1.5G spectrum : The absorption in the different encapsulants is shown in dark blue.

We produce p-type passivated emitter and rear cells (PERC) and take two cells with 20.7% efficiency, that have nearly identical current-voltage (*IV*) and EQE characteristics. To investigate the impact of both EVA types we encapsulate those cells in a module using the same materials except for the EVA encapsulation. After encapsulation we measure both modules using a type AAA flasher, that contains hardly any light for wavelengths shorter than 360 nm. Therefore, we correct for the flasher's spectral mismatch afterwards the results show the module encapsulated with EVA_{UV-T} generates (1.4±0.2)% more current than the one with EVA_{Conv}. The experimental results are presented in greater detail in Ref. [8].

4. Monthly energy yield under realistic irradiation

In order to allow for a realistic representation of daylight within a simulation, its spectral and angular distribution has to be modelled. We utilize an in-house developed mean annual daylight model [23] which is based on irradiances that we measured over 14 years (1992 – 2006) in Hamelin, Germany. The measurements were performed using a pair of photopyranometers to obtain the values of horizontal global and diffuse irradiance with a temporal resolution of 5 minutes. Our model includes the impact of the sun's position and clouds on the angular and spectral distribution. However, scattering of light is treated wavelength independent. This means that the spectral impact of e.g. aerosols or seasonal changes in the atmosphere composition are neglected. The result of our approach is a mean annual daylight distribution that models the celestial hemisphere by a partition into solid-angle intervals of 5° azimuth and 5° altitude. Each of these intervals contains its own spectral distribution of diffuse and direct light.

Figure 4 shows the ray tracing results of a module with conventional EVA (left) and with EVA_{UV-T} (right) under these realistic irradiation conditions. The intensity of our realistic light source is scaled to the 1000 W/m² of AM1.5G spectrum for better comparison. In both modules the losses at each wavelength are increased. The conventional EVA_{Conv} absorbs most of the light in the UV wavelength range below 380 nm, here shown in dark blue. In contrast, the module with EVA_{UV-T} (right) generates more current in this region, but also the losses in the

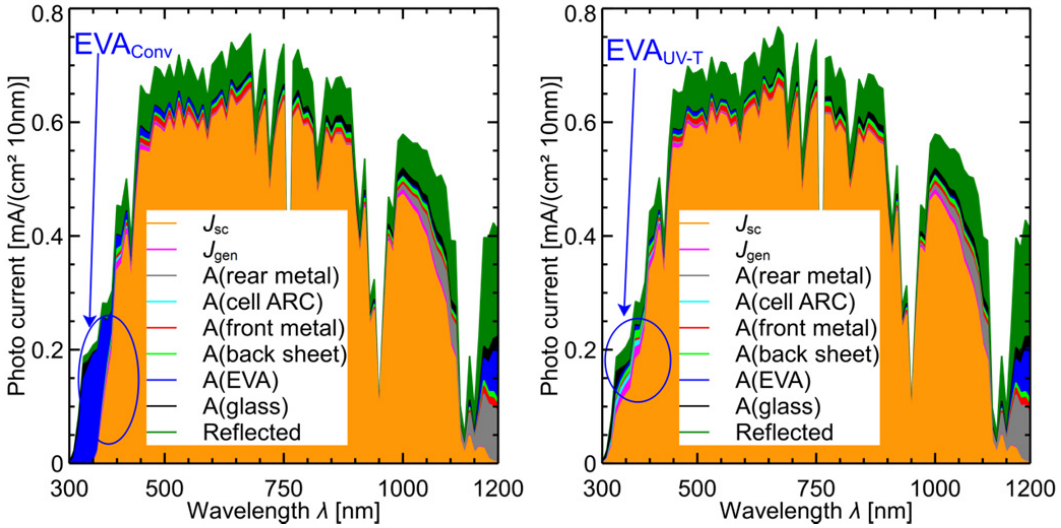

Fig. 4. Optical loss analysis under realistic irradiation of the PV modules with EVA$_{Conv}$ (left) and EVA$_{UV-T}$ (right): The absorption in the different encapsulants is shown in dark blue.

back sheet (light green), in the cell ARC (cyan) and losses due to the collection efficiency (pink) are increased in this region. Integration over all wavelengths results in a gain (1.9±0.4)% in J_{sc} by using UV transparent over of conventional EVA. This increase is mainly caused by the blue shift in this realistic irradiation spectrum compared to the AM1.5G spectrum. In terms of the average photon energy (APE) [24] our realistic light source spectrum has a APE of 1.85 eV (300-1200 nm), while the AM1.5G has an APE of 1.8 eV (300-1200 nm) thus we have a blue shift of 2.9%. Other measurements of irradiation spectrums over the time range of at least one year have reported higher blue shifts of the APE of up to 4-6% [24] [25] [26]. Thus when considering UV optimization of PV modules one should consider realistic spectrums.

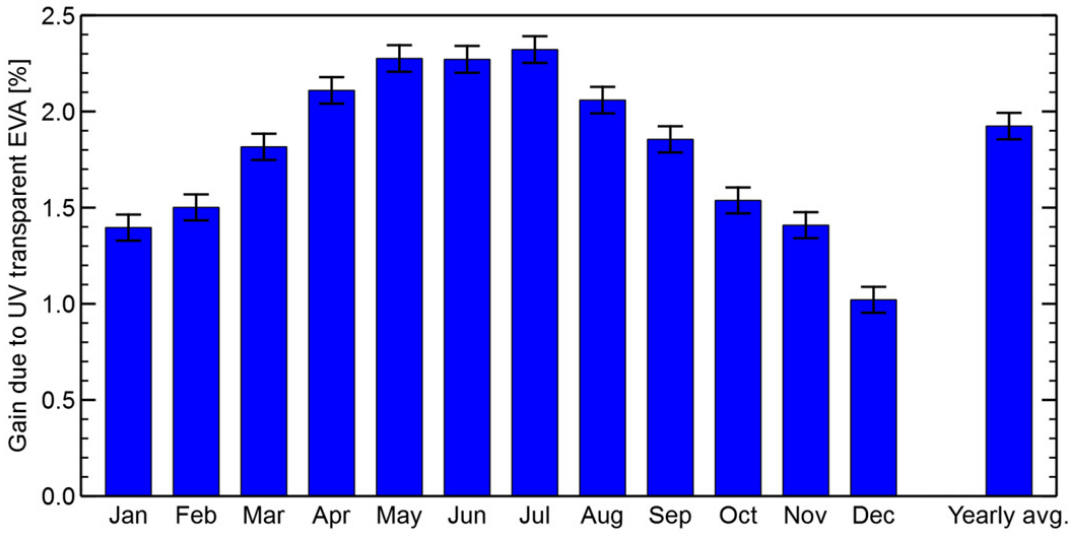

Fig. 5. Monthly simulated gain in J_{sc} when replacing conventional EVA$_{Conv}$ with UV transparent EVA$_{UV-T}$ using realistic irradiation conditions.

In contrast to previous analyses [23], we also simulate each month separately to reveal seasonal impacts. Figure 5 shows the simulated monthly gain when replacing conventional EVA_{Conv} with UV transparent $EVA_{UV\text{-}T}$. The gain is largest in the summer time with up 2.3%. Consequently, we also have a lower gain in the winter months.

These findings clearly show the necessity of considering realistic conditions when evaluating the performance of different materials.

5. Summary and conclusion

We discussed the optical properties of UV transparent and conventional ethylene vinyl acetate (EVA). Simulation and experiments at standard testing conditions with AM1.5G spectra predict a gain of about 1.3 to 1.4% in J_{sc} by using UV transparent instead of conventional EVA. Our ray tracing results show that more UV light is absorbed in the back sheet and the cell's anti reflective coating in a PV module with $EVA_{UV\text{-}T}$. Thus UV stability of back sheets and solar cells becomes more important when using EVA with enhanced UV-transmission.

To determine the gain under more realistic irradiation conditions with respect to angular and spectral distribution we performed ray tracing simulations. These simulations reveal an increase of 1.9% in the yearly average, which is strongest in the summer months with an increase of up to 2.3%. These results demonstrate the importance to use more realistic irradiation conditions than STC in order to evaluate the potential of future technologies in photovoltaics.

Acknowledgements

This work was supported by the German Federal Ministry for Economic Affairs and Energy through the "PERC2Module" project under Contract 0325641. We would also like to thank Martin Wolf, Tobias Gandy, Sarah Spätlich, Ulrike Sonntag, Till Brendemühl for the cell production.

References

[1] Hahn G. Status of selective emitter technology. 5th WCPEC 2010;1091–1096.
[2] Mcintosh KR, Cotsell JN, Cumpston JS, Norris AW, Powell NE, Ketola BM. An optical comparison of silicone and EVA encapsulants for conventional silicon PV modules: A ray-tracing study. 34th IEEE PVSC 2009; 544–549.
[3] Zhang S, Deng W, Pan X, Jiao H, Chen D, Huang H, Cui Y, Feng J, Zhong M, Chen Y, Altermatt PP, Feng Z, Verlinden P. 335 Watt World Record P-type Mono-crystalline Module With 20.6 % Efficiency PERC Solar Cells. 41st IEEE PVSC 2015.
[4] ISFH press release. 20.2% module efficiency with industrial processed passivated emitter and rear solar cells. 20.1.2016.
[5] Khoo YS, Walsh TM, Lu F, Aberle AG. Method for quantifying optical parasitic absorptance loss of glass and encapsulant materials of silicon wafer based photovoltaic modules. Sol. Energy Mater. Sol. Cells 2012;102:153–158.
[6] Schmid C, Chapon J, Kinsey G, Bokria J, Woods J. Impact of high light transmission EVA-based encapsulant on the performance of PV modules. 27th EUPVSEC 2012; p. 3494.
[7] Haedrich I, Eitner U, Wiese M, Wirth H. Unified methodology for determining CTM ratios: Systematic prediction of module power. Sol. Energy Mater. Sol. Cells 2014;131(7):14–23.
[8] Vogt MR, Holst H, Schulte-Huxel H, Blankemeyer S, Hinken D, Witteck R, Winter M, Min B, Schinke C, Ahrens I, Köntges M, Bothe K, Brendel R. To be Publ. 2016.
[9] Agilent-Technologies. Agilent diffuse reflectance accesories (DRAs) for the cary 4000/5000/6000i UV-VIS-NIR spectrometers 2013. http://www.chem.agilent.com/Library/flyers/Public/5991-1717EN_PromoFlyer_UV_DRA.pdf.
[10] Woollam JA. Manual for WVASE32 2010.
[11] Nagel H, Aberle AG, Hezel R. Optimised antireflection coatings for planar silicon solar cells using remote PECVD silicon nitride and porous silicon dioxide. Prog. Photovoltaics Res. Appl. 1999;4(7):245–260.
[12] Schinke C, Christian Peest P, Schmidt J, Brendel R, Bothe K, Vogt MR, Kröger I, Winter S, Schirmacher A, Lim S, Nguyen HT, MacDonald D. Uncertainty analysis for the coefficient of band-to-band absorption of crystalline silicon. AIP Adv. 2015;5(6):067168.
[13] Vogt MR, Hahn H, Holst H, Winter M, Schinke C, Kontges M, Brendel R, Altermatt PP. Measurement of the Optical Constants of Soda-Lime Glasses in Dependence of Iron Content and Modeling of Iron-Related Power Losses in Crystalline Si Solar Cell Modules. IEEE JPV 2016;6(1):111–118.
[14] Thaworn K, Buahom P, Areerat S. Effects of Organic Peroxides on the Curing Behavior of EVA Encapsulant Resin. Open J. Polym. Chem. 2012;2(2):77–85.

[15] Holst H, Winter M, Schulte-Huxel H, Blankemeyer S, Witteck R, Vogt MR, Booz T, Distelrath F, Köntges M, Bothe K, Brendel R. Increased light harvesting by structured cell interconnectors: an optical ray tracing study under realistic daylight conditions. SiliconPV 2016.
[16] Witteck R, Schulte-Huxel H, Holst H, Hinken D, Vogt MR, Blankemeyer S, Köntges M, Bothe K, Brendel R. Optimizing the solar cell front side metallization and the cell interconnection for high module power output. SiliconPV 2016.
[17] Vogt MR. Development of Physical Models for the Simulation of Optical Properties of Solar Cell Modules. Leibniz Universität Hannover. PhD thesis 2015.
[18] Palik ED. Handbook of Optical Constants of Solids. Academic Press Inc. 1985.
[19] Shiles E, Sasaki T, Inokuti M, Smith DY. Self-consistency and sum-rule tests in the Kramers-Kronig analysis of optical data: Applications to aluminum. Phys. Rev. B 1980;22(4):1612–1628.
[20] Holst H, Winter M, Vogt MR, Bothe K, Köntges M, Brendel R, Altermatt PP. Application of a new ray tracing framework to the analysis of extended regions in Si solar cell modules. Energy Procedia 2013;38:86–93.
[21] Winter M, Vogt MR, Holst H, Altermatt PP. Combining structures on different length scales in ray tracing: analysis of optical losses in solar cell modules. Opt. Quantum Electron 2015;47(6):1373–1379.
[22] Synopsys Incorparation. Sentaurus Device. Mountain View, CA, USA.
[23] Winter M, Holst H, Vogt MR, Altermatt PP. Impact of realistic illumination on optical losses in Si solar cell modules compared to standard testing conditions. 31st EU PVSEC 2015;1869–1874.
[24] Betts TR. Investigation of Photovoltaic Device Operation under Varying Spectral Conditions. Loughborough University. PhD thesis 2004.
[25] Zinsser B. Jahresenergieerträge unterschiedlicher Photovoltaik-Technologien bei verschiedenen klimatischen Bedingungen. Universität Stuttgart, 2011.
[26] Behrendt T, Kuehnert J, Hammer A, Lorenz E, Betcke J, Heinemann D. Solar spectral irradiance derived from satellite data: A tool to improve thin film PV performance estimations?. Sol. Energy 2013; 98:100–110.